Monthly Notices
of the
ROYAL ASTRONOMICAL SOCIETY

MNRAS **448,** 464–483 (2015) doi:10.1093/mnras/stv002

Using broad-band photometry to examine the nature of long secondary periods in red giants

M. Takayama,[1⋆] P. R. Wood[2] and Y. Ita[1]

[1]*Astronomical Institute, Graduate School of Science, Tohoku University, Sendai, Miyagi 980-8578, Japan*
[2]*Research School of Astronomy and Astrophysics, Australian National University, Cotter Road, Weston Creek, ACT 2611, Australia*

Accepted 2014 December 28. Received 2014 December 28; in original form 2014 August 5

ABSTRACT

Long-term *JHK* light curves have recently become available for large numbers of the more luminous stars in the Small Magellanic Cloud (SMC). We have used these *JHK* light curves, along with OGLE (Optical Gravitational Lensing Experiment) *V* and *I* light curves, to examine the variability of a sample of luminous red giants in the SMC which show prominent long secondary periods (LSPs). The origin of the LSPs is currently unknown. In oxygen-rich stars, we found that while most broad-band colours (e.g. $V-I$) get redder when an oxygen-rich star dims during its LSP cycle, the $J-K$ colour barely changes and sometimes becomes bluer. We interpret the $J-K$ colour changes as being due to increasing water vapour absorption during declining light caused by the development of a layer of dense cool gas above the photosphere. This result and previous observations which indicate the development of a chromosphere between minimum to maximum light suggest that the LSP phenomenon is associated with the ejection of matter from the stellar photosphere near the beginning of light decline. We explore the possibility that broad-band light variations from the optical to the near-infrared regions can be explained by either dust absorption by ejected matter or large spots on a rotating stellar surface. However, neither model is capable of explaining the observed light variations in a variety of colour–magnitude diagrams. We conclude that some other mechanism is responsible for the light variations associated with LSPs in red giants.

Key words: circumstellar matter – infrared: stars.

1 INTRODUCTION

All luminous red giants appear to be variables and they are generally known as long period variables (LPVs). They vary with periods which fall on at least eight period–luminosity sequences which have been labelled A′, A, B, C′, C, D, E and F (Wood et al. 1999; Ita et al. 2004; Soszyński et al. 2004; Tabur et al. 2010; Soszyński & Wood 2013). Sequences A′–C and F are thought to consist of stars pulsating in the radial fundamental and overtone modes and the non-radial dipole and quadrupole modes (Wood et al. 1999; Ita et al. 2004; Soszyński & Wood 2013; Takayama, Saio & Ita 2013; Stello et al. 2014). These stars have been classified as Miras, Semi-Regulars and OGLE (Optical Gravitational Lensing Experiment) small amplitude red giants (Wood et al. 1999; Soszyński et al. 2004, 2007). On the other hand, sequence E is known to consist of close binary system showing ellipsoidal and eclipsing variability (Wood et al. 1999; Derekas et al. 2006; Soszyński 2007).

The last sequence, called sequence D, exhibits the longest periods of all the sequences. Sequence D stars show photometric variations with periods of ∼400–1500 d and they also show other variations with a shorter period that usually correspond to the period of sequence B. In these stars, the shorter period is called the primary period and the longer period corresponding to sequence D is known as a long secondary period (LSP). LSP stars have been found within the (Large Magellanic Cloud) LMC, Small Magellanic Cloud (SMC) and Galactic populations of LPVs. In fact, approximately 25–50 per cent of luminous red giants have been found to show LSPs in MACHO and OGLE data (Wood et al. 1999; Soszyński et al. 2007; Fraser, Hawley & Cook 2008). However, the origin of the LSP phenomenon is still unknown and many explanations have been suggested. Some of these are now highlighted.

The most straightforward explanation is pulsation. However, all pulsation explanations have problems. Since, at the given luminosity, the typical LSP is approximately four times longer than the period of a Mira (on sequence C), and since the Miras are known to be pulsating in the radial fundamental mode, an explanation in terms of normal-mode radial pulsation is not possible. Non-radial g-mode

⋆ E-mail: m.takayama@astr.tohoku.ac.jp

pulsation was proposed as the explanation of the LSP phenomenon by Wood et al. (1999) since g-mode periods can be longer than the radial fundamental mode period. However, because red giants have a large convective envelope and only a thin outer radiative layer where g modes could develop, the amplitude of g modes should be too small to correspond to the observed light and radial velocity amplitudes of LSP stars (Wood, Olivier & Kawaler 2004).

Some researchers have also argued for a close binary hypothesis (like sequence E) to explain the LSP phenomenon. Soszyński (2007) found at least 5 per cent of LSP stars showed ellipsoidal or eclipse-like variability. He also noted, as did Derekas et al. (2006), that if the sequence E ellipsoidal variable were plotted using the orbital period rather than the photometric period (half the orbital period), then sequences D and E overlapped on the period–luminosity diagram. However, the large amplitude of many LSP light curves (up to 1 mag) would require a close pair of eclipsing red giants, very unlikely in itself, and this would lead to alternating deep and shallow minima which are not seen. On the other hand, Wood et al. (1999) found that many light curves due to the LSPs show faster decline and slower rise and they proposed that a binary with a companion surrounded by a comet-shaped cloud of gas and dust could give rise to those light-curve features. Various observational and numerical results have conflicted with the binary hypothesis. Hinkle et al. (2002) observed radial velocity variations in six local red giants with LSPs and found that the velocity curves all had a similar shape. For eccentric binaries with a random longitude of periastron, the light-curve shape should vary from star to star. The lack of such variability led Hinkle et al. (2002) to reject the binary explanation for LSPs. Wood et al. (2004) and Nicholls et al. (2009) obtained radial velocity curves for stars in the Galaxy and LMC and they argued that the small typical full velocity amplitude of $\sim$3.5 km s^{-1} meant that all binary companions would need a mass near 0.09 $M_{\odot}$. Since companions of this mass are rare around main-sequence stars, it seems unlikely that the 25–50 per cent of red giants which show LSPs could have a companion of this mass.

Star-spots due to magnetic activity on asymptotic giant branch (AGB) stars have been proposed by some researchers (e.g. Soker & Clayton 1999) and a rotating spotted star has been suggested as an explanation of the LSPs. Possible evidence for magnetic activity in stars with LSPs is provided by the existence of Hα absorption lines whose strength varies with the LSP (Wood et al. 2004). However, from observations, Olivier & Wood (2003) found that the rotation velocity of LSP stars is typically less than 3 km s^{-1} and they noted that this rotation velocity is too small to explain the periods of less than 1000 d which are often observed for the LSP. For example, a 3 km s^{-1} rotation velocity gives rise to the period of 2868 d for an AGB star with a $\sim$170 $R_{\odot}$. A way to overcome this objection would be to have multiple star-spots. In another study, Wood et al. (2004) found that with a simple blackbody model, it was difficult for a rotating spotted star to simultaneously reproduce both the amplitude and colour variation observed in the MACHO observations of stars with LSPs. The use of model atmospheres rather than blackbodies, and allowing for limb darkening, could alter this conclusion.

The giant convective cell model is a relatively new explanation of the LSP phenomenon (Stothers 2010). This model is somewhat similar to the rotating spot model in that it involves variable amounts of the visible stellar surface having a temperature cooler than normal. The photometric variations seen in both the rotating spot model and the giant convective cell model should be similar.

Another potential origin for the LSP is a variable amount of circumstellar dust. Wood et al. (1999) proposed that the periodic dust formation found in the circumstellar regions of theoretical models of AGB stars by Winters et al. (1994) and Höfner, Feuchtinger & Dorfi (1995) could give rise to the light variation of the LSPs. Evidence for dust around red giants with LSPs was found by Wood & Nicholls (2009) who showed that LSP stars tend to have a mid-infrared (mid-IR) excess. On near- to mid-IR colour–magnitude diagrams, the LSP stars lie in a region similar to that occupied by R Coronae Borealis (RCB) stars which are known to be surrounded by patchy circumstellar dust clouds. This result suggests that the variation of LSP stars might be due to the ejection of dust shells that may be patchy. Similarly, in studying the effect of dust ejection on MACHO colours and magnitudes, Wood et al. (2004) noted that patchy dust clouds seemed to be required in order to reproduce the observed colour–magnitude variations.

In this paper, we utilize new long-term near-infrared (near-IR) JHK_s light curves of stars in the SMC obtained with the Simultaneous-3color InfraRed Imager for Unbiased Survey (SIRIUS) camera on the InfraRed Survey Facility (IRSF) 1.4 m telescope (Ita et al., in preparation). We combine the JHK_s observations with V and I monitoring of SMC stars by OGLE (Soszyński et al. 2011). Using this combined data, we examine light and colour variations of LSP stars over a wide wavelength range. We then test models involving dust ejection or variable spots to see if they can reproduce the observed light and colour variations over the wide wavelength range. For our computations, the DUSTY code (Ivezić, Nenkova & Elitzur 1999) is used to model the effects of ejected dust and the 2012 version of the Wilson–Devinney code (Wilson & Devinney 1971) is used to model the effects on the light and colour of a spotted star.

2 THE OBSERVATIONAL DATA

2.1 The near-IR data

A long-term multiband near-IR photometric survey for variable stars in the Large and Small Magellanic Clouds has been carried out at the South African Astronomical Observatory at Sutherland (Ita et al., in preparation). The SIRIUS camera attached to the IRSF 1.4 m telescope was used for this survey and more than 10 yr of observations in the near-IR bands J(1.25 μm), H(1.63 μm) and K_s(2.14 μm) band were obtained. In this work, we select the SMC stars from the SIRIUS data base. Variable and non-variable stars in an area of 1 deg^2 in the central part of the SMC have been observed about 99–126 times in the period 2001–2012 and a total of 340 147, 301 841 and 215 463 sources were identified in J, H and K_s, respectively. We note that the photometric detection range of the SIRIUS camera is about 8–18 mag in the K_s band. A total of 12 008 variable sources of all kinds were detected of which 4533 were detected in all three wavebands (data release ver. 130501; Ita et al., in preparation).

2.2 The optical data

We obtained the V- and I-band time series of SMC red giants from the OGLE project (Soszyński et al. 2011). Typically, about 1000 observing points were obtained in the I band by OGLE-II+III while a much smaller number of about 50–70 points were obtained in the V band.

Soszyński et al. (2011) divided the LPVs into LSP and non-LSP stars according to their positions in the period–luminosity relations for variable red giants. We found nearly 700 LSP stars in the area of the IRSF infrared survey. In order to determine if an LSP star is oxygen-rich or carbon-rich, we initially adopted the classification

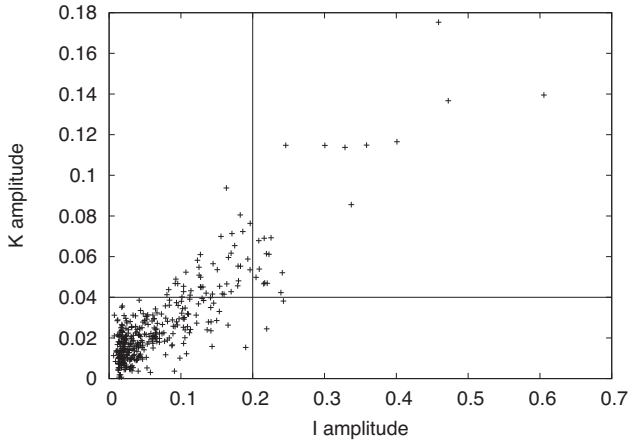

Figure 1. The relation between the I- and K_s-band full amplitude of 298 oxygen-rich stars and 88 carbon stars. The stars selected for detailed study have I amplitude greater than 0.2 mag and K_s amplitude greater than 0.04 mag.

method introduced by Soszyński et al. (2011). The stars we examined in detail had their oxygen-rich or carbon-rich status checked against optical spectral classifications in the literature.

2.3 The combined near-IR and optical data

By combining the SIRIUS data with the OGLE data, we obtained 298 oxygen-rich LSP stars and 88 carbon-rich LSP stars in the region monitored by the SIRIUS camera. For all sample stars, a small number of apparent bad data points were removed from each time series. Then, by using a first-order Fourier fit to the I-band time series, we obtained the period and amplitude corresponding to the largest amplitude mode of the light curves. In all cases, the obtained periods and amplitudes were almost identical to those in the OGLE-III catalogue (Soszyński et al. 2011). Using the period from the fit to the I light curve, a fit was also made to the K_s light curve in order to derive its amplitude.

Since our aim is to look for and to model colour and magnitude changes, we need the observed changes to be significantly larger than the noise in the data. The limiting factor in this study is noise in the near-IR data. We concentrate on the brightest stars with $K_s < 13$ and for them the useful lower limit for clearly apparent K_s-band variation is about 0.04 mag. Similarly, we set a useful lower limit for the I-band variation of about 0.2 mag. Fig. 1 shows the full amplitude of the observed LSP stars in the I and K_s bands. This figure shows the selected stars, which having full amplitudes larger than 0.04 mag in K_s and 0.2 mag in I. This selection gave us a sample of 7 oxygen-rich stars and 14 carbon stars for analysis. The spectral types of our sample stars obtained from the OGLE photometry agree with the classifications in the Set of Identifications, Measurements and Bibliography for Astronomical Data (SIMBAD) astronomical data base where the spectral types were obtained from spectroscopic determinations. The properties of these stars at maximum light are listed in Table 1.

Near-IR JHK_s photometric data as a function of Julian date (JD) for a sample of 7 oxygen-rich stars and 14 carbon stars are published along with this paper. The file name of the time series data indicates star-name and waveband, like 'OGLE-SMC-LPV-07852.J.dat'. Table 2 shows time series for a sample of the LSP star, which consists of seven columns as follows.

Column 1 : Julian day.

Column 2 : calibrated (2MASS referenced) magnitude.

Column 3 : error in deferential image analysis in magnitude.

Column 4 : error in reference magnitude.

Column 5 : error in conversion offset in magnitude.

Column 6 : name of the survey region in which the variable star is detected.

Column 7 : name of the survey subregion in which the variable star is detected.

For more details, see Ita et al. (in preparation).

Table 1. Basic parameters of the program stars at maximum light.

Name	RA	Dec.	V (mag)	I (mag)	J (mag)	H (mag)	K_s (mag)	L ($L_\odot$)	T_{BB} (K)	T_{eff} (K)	P_{LSP} (d)	Sp. type
OGLE-SMC-LPV-07852	12.402 540	−72.970 75	16.60	14.34	12.91	12.05	11.73	4617	2803	3434	645	O
OGLE-SMC-LPV-09856	13.186 620	−72.951 78	16.49	14.37	12.96	12.10	11.86	4408	2928	3558	615	O
OGLE-SMC-LPV-10774	13.530 120	−72.479 89	–	14.98	13.73	12.81	12.57	2170	2844	3474	396	O
OGLE-SMC-LPV-12332	14.166 840	−73.073 89	–	14.26	12.95	12.08	11.82	4455	2887	3517	632	O
OGLE-SMC-LPV-14045	14.987 085	−72.949 36	17.50	15.13	13.72	12.79	12.57	2197	2865	3495	390	O
OGLE-SMC-LPV-14715	15.332 205	−72.863 69	–	14.27	12.92	12.03	11.75	4544	2815	3445	601	O
OGLE-SMC-LPV-14781	15.361 920	−72.856 78	16.48	14.62	13.30	12.44	12.23	3245	2991	3620	469	O
OGLE-SMC-LPV-08199	12.555 540	−73.186 97	17.75	14.90	13.29	12.27	11.64	3745	2203	2792	767	C
OGLE-SMC-LPV-08280	12.583 995	−72.805 33	16.36	13.78	12.33	11.36	10.93	7922	2490	3106	1008	C
OGLE-SMC-LPV-09341	12.990 495	−73.202 56	–	13.92	12.48	11.63	11.26	6419	2734	3362	1081	C
OGLE-SMC-LPV-10109	13.281 915	−73.129 92	16.08	13.84	12.52	11.60	11.20	6411	2592	3215	964	C
OGLE-SMC-LPV-12653	14.317 380	−72.801 28	–	14.83	13.10	12.03	11.44	4465	2200	2789	1356	C
OGLE-SMC-LPV-13340	14.654 580	−72.446 25	16.28	14.12	12.59	11.66	11.28	6003	2606	3230	1014	C
OGLE-SMC-LPV-13557	14.755 710	−72.469 08	16.31	13.91	12.45	11.54	11.13	6876	2592	3215	1032	C
OGLE-SMC-LPV-13748	14.847 210	−73.049 00	–	14.69	13.09	12.11	11.67	3977	2468	3082	925	C
OGLE-SMC-LPV-13802	14.871 165	−72.657 50	17.08	14.19	12.69	11.71	11.16	6085	2334	2936	1011	C
OGLE-SMC-LPV-13945	14.946 045	−72.710 94	–	14.06	12.63	11.73	11.29	5872	2560	3180	927	C
OGLE-SMC-LPV-14084	15.004 245	−72.898 39	16.30	14.27	12.74	11.83	11.53	5042	2759	3388	799	C
OGLE-SMC-LPV-14159	15.048 705	−72.668 22	–	14.42	12.96	12.04	11.57	4406	2495	3112	913	C
OGLE-SMC-LPV-14829	15.382 875	−73.099 19	15.69	13.70	12.37	11.54	11.21	6950	2839	3469	780	C
OGLE-SMC-LPV-14912	15.434 040	−73.295 06	–	14.49	12.92	11.91	11.31	5135	2244	2837	722	C

Notes. T_{BB} is the blackbody temperature derived from $J - K_s$ while T_{eff} is the effective temperature derived from $J - K_s$ using the formula in Bessell, Wood & Evans (1983). Luminosities L were derived by applying a bolometric correction to K_s (see Section 4.1).

Table 2. The first 10 records from the time series data for a variable source in the *J* band (OGLE-SMC-LPV-07852). The seven columns are explained in the text. The full version of this table is available as online material.

Column 1 (d)	Column 2 (mag)	Column 3 (mag)	Column 4 (mag)	Column 5 (mag)	Column 6	Column 7
245 2092.635 160	12.930	0.003	0.019	0.003	SMC0050-7250	C
245 2212.344 921	12.959	0.002	0.019	0.003	SMC0050-7250	C
245 2213.302 422	12.958	0.003	0.019	0.003	SMC0050-7250	C
245 2214.397 972	12.940	0.002	0.019	0.003	SMC0050-7250	C
245 2246.289 626	12.991	0.003	0.019	0.003	SMC0050-7250	C
245 2285.324 709	13.007	0.003	0.019	0.003	SMC0050-7250	C
245 2298.305 372	12.974	0.003	0.019	0.003	SMC0050-7250	C
245 2390.680 728	12.931	0.002	0.019	0.003	SMC0050-7250	C
245 2411.689 245	12.948	0.002	0.019	0.003	SMC0050-7250	C
245 2415.634 797	12.965	0.003	0.019	0.003	SMC0050-7250	C

3 SEPARATING THE LSP VARIATION FROM THE PRIMARY PERIOD VARIATION

Light curves of all LSP stars show variations with the period corresponding to sequence D and also variations with the primary period, which mainly corresponds to sequence B. Therefore, in order to study the LSP variation only, we need to separate each light curve into the components due to variation with the LSP and variation with the primary period. The separation method we used is now described.

At first, we adopted a reference time t_0 and then delimited the light curve into time intervals equal to the size of the LSP (P), with t_0 as the start of an interval. Then we fitted the observed data points in each interval independently using a second-order Fourier series F_0 with the period equal to that of the LSP,

$$F_0(t) = A_0 + \sum_{i=1}^{2} a_0 \sin\left(2\pi i \frac{t-t_0}{P}\right) + b_0 \cos\left(2\pi i \frac{t-t_0}{P}\right).$$

The fit was performed on independent intervals of length P rather than the full light-curve interval because the light curves of LSP stars vary substantially from cycle to cycle of the LSP. Furthermore, in order to minimize the dependence of the final fit on the adopted value of t_0, the fit was made using four values for t_0, τ_0, τ_1, τ_2 and τ_3, with each of these values increasing by $\frac{1}{4}P$, giving fits $F_0(t)$, $F_1(t)$, $F_2(t)$ and $F_3(t)$, respectively. In this study, τ_0 corresponds to JD245 0000. A requirement for a fit to be made was that there be at least six points in each of the first and second halves of the fit interval. If such points were not available, no fit was made. The final adopted fit $F(t)$ at the observed times is given by

$$F(t) = \frac{1}{4}\sum_{j=0}^{3} F_j(t).$$

When there were fewer than four fits, the average was taken over the number of fits available. An example of the final light-curve fits for each band in a representative star is shown in Fig. 2.

As one can see from Fig. 2, observation times of the OGLE *I* band usually differed from those of the OGLE *V* band and the SIRIUS *J*, *H* and K_s bands, the latter being taken simultaneously. The *I*-band observations are always the most frequent. In our analysis, we will examine colours relative to the *I*-band magnitude. In order to derive the colours and *I*-band magnitudes at simultaneous dates, the *I*-band fits to the LSP variations were used. Magnitudes and colours were derived from the fits at observation times of the *V* band and the K_s band. As noted above, fits are not available at all times in a given band.

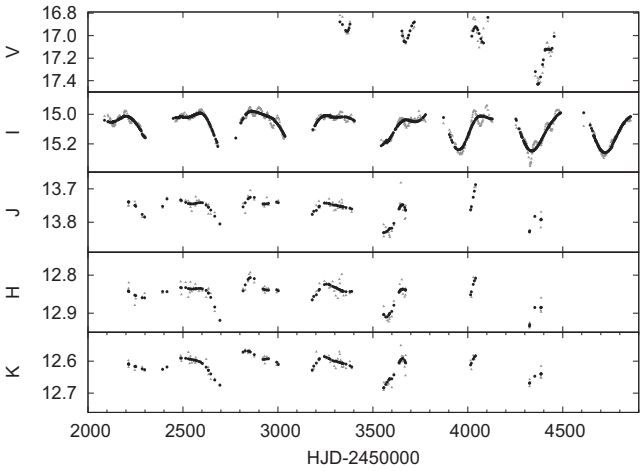

Figure 2. The complete light curves of OGLE-SMC-LPV-10774 (P=396 d) in the bands *VIJHK*. The raw data points are shown as small filled grey triangles while the fit values are shown as large filled black circles.

4 MODELING THE LSP MAGNITUDE AND COLOUR VARIATIONS

We will now create models for the magnitude variations in various bands associated with LSPs in order to see if the assumed models are consistent with the observations. The two models we examine are obscuration by dust and the variation of spots on a star.

4.1 The dust model

One possible explanation of the LSP phenomenon is episodic circumstellar dust absorption. Here we assume that the central star ejects mass for several hundred days in each LSP cycle, leading to the formation of thin spherical mass shells. Dust grains which form in the ejected matter will be carried along with the expanding mass shells leading to dimming of the light from the central star. We assume that the dust shells are ejected spherically although this is not an essential aspect of the dust model for the optical and near-IR bands which we are examining since thermal emission in these bands is not strong.

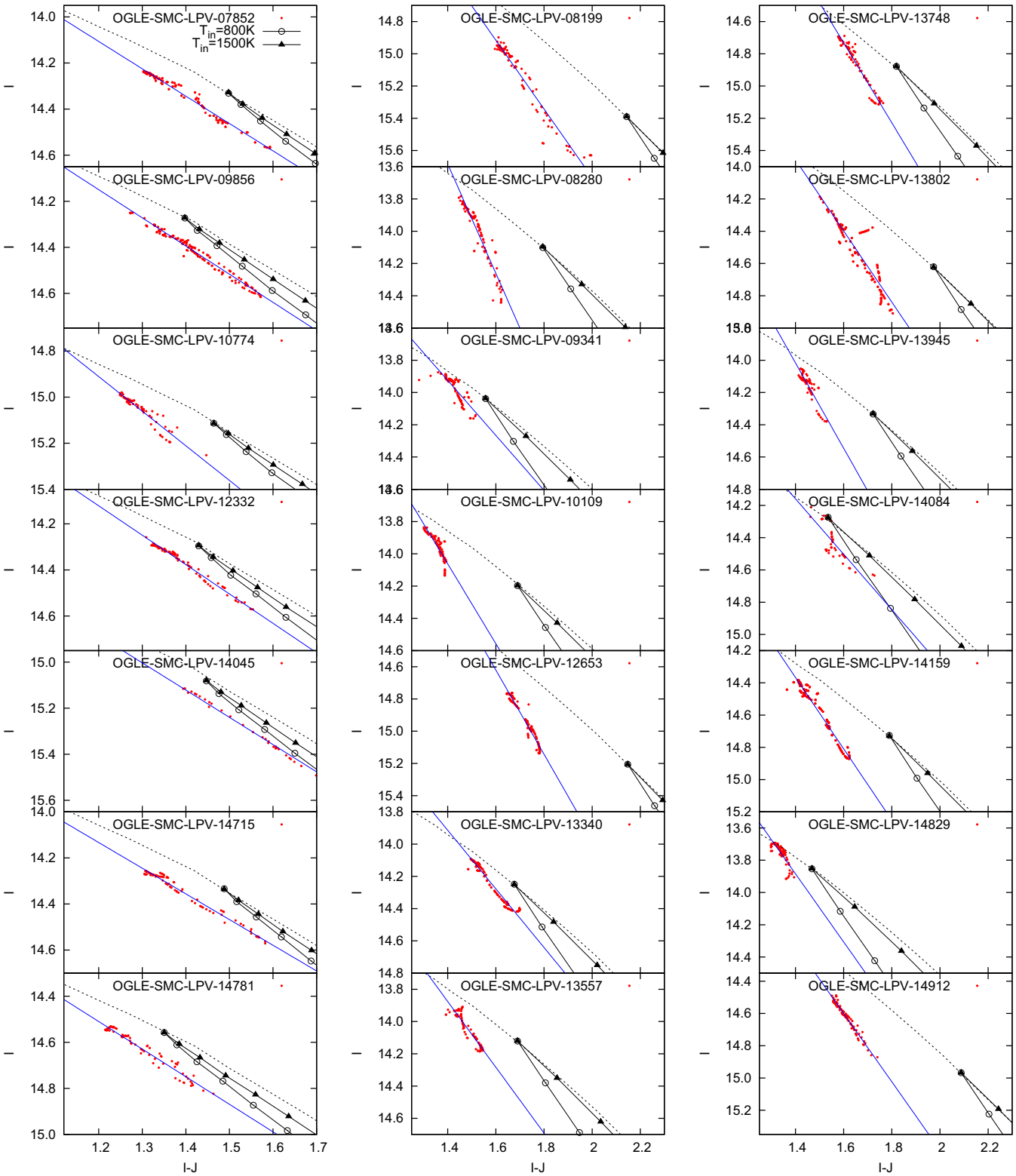

Figure 3. Comparisons of observations with models of expansion velocity 15 km s^{-1}. The 7 panels of the left-hand column represent the I and $I-J$ variations for the oxygen-rich stars and the 14 panels of the middle and right-hand columns are for the carbon stars. The red points show the LSP variations obtained from Fourier fits to the observed light curves. The blue lines show least-squares fit to these points (the line is omitted if the relative error in the slope is more than 0.2). The black continuous lines with open circles show the magnitude and colour variations for models with an inner dust shell temperature of 800 K while the triangles are for models with an inner dust shell temperature of 1500 K. The top end of each curve corresponds to shell optical depth $\tau_V = 0$ and the points are spaced at intervals of 0.5 in $\tau_V = 0$. The black dotted lines show the locus of un-extincted blackbodies of different temperatures and the constant luminosity given in Table 1 for each star. Note that the scale of the vertical axis is the same for all oxygen-rich stars and for all carbon stars.

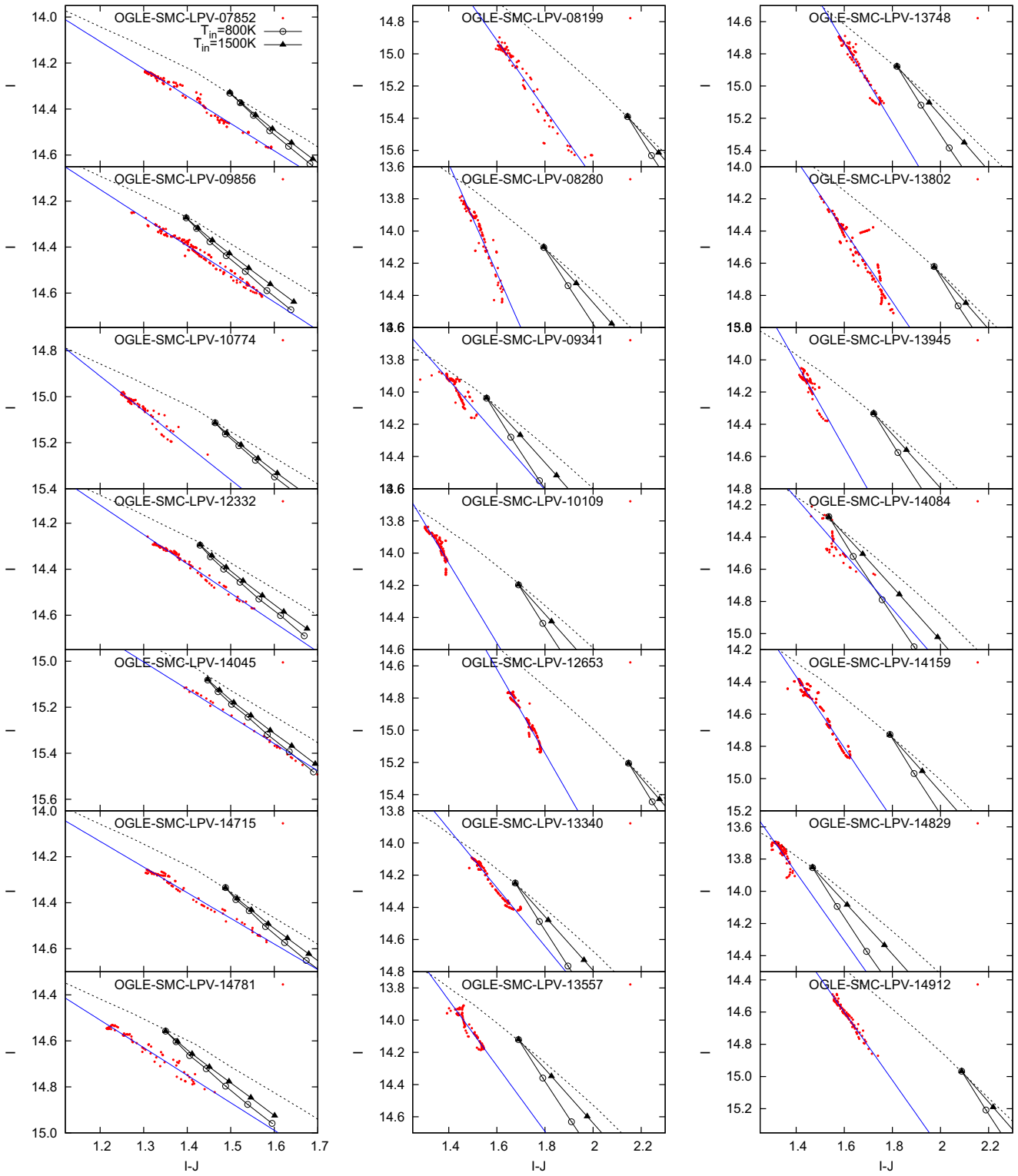

Figure 4. The same as Fig. 3 but for models with an expansion velocity of 220 km s^{-1}.

The amount of dimming of a star due to circumstellar dust depends on the optical depth through the dust. For a spherical dust shell with an outer radius $R_{\rm out}$ (corresponding to the start of a mass ejection episode), an inner radius $R_{\rm in}$ (corresponding to the end of a mass ejection episode, or the dust formation radius in a newly-forming inner shell), a constant expansion velocity v and a mass ejection rate $\dot{M}$, the optical depth τ_λ through the shell is given by (e.g. Groenewegen & de Jong 1993)

$$\tau_\lambda \propto \frac{\dot{M}\Psi Q_\lambda/a}{v\rho_{\rm g}}\left(\frac{1}{R_{\rm in}}-\frac{1}{R_{\rm out}}\right), \quad (1)$$

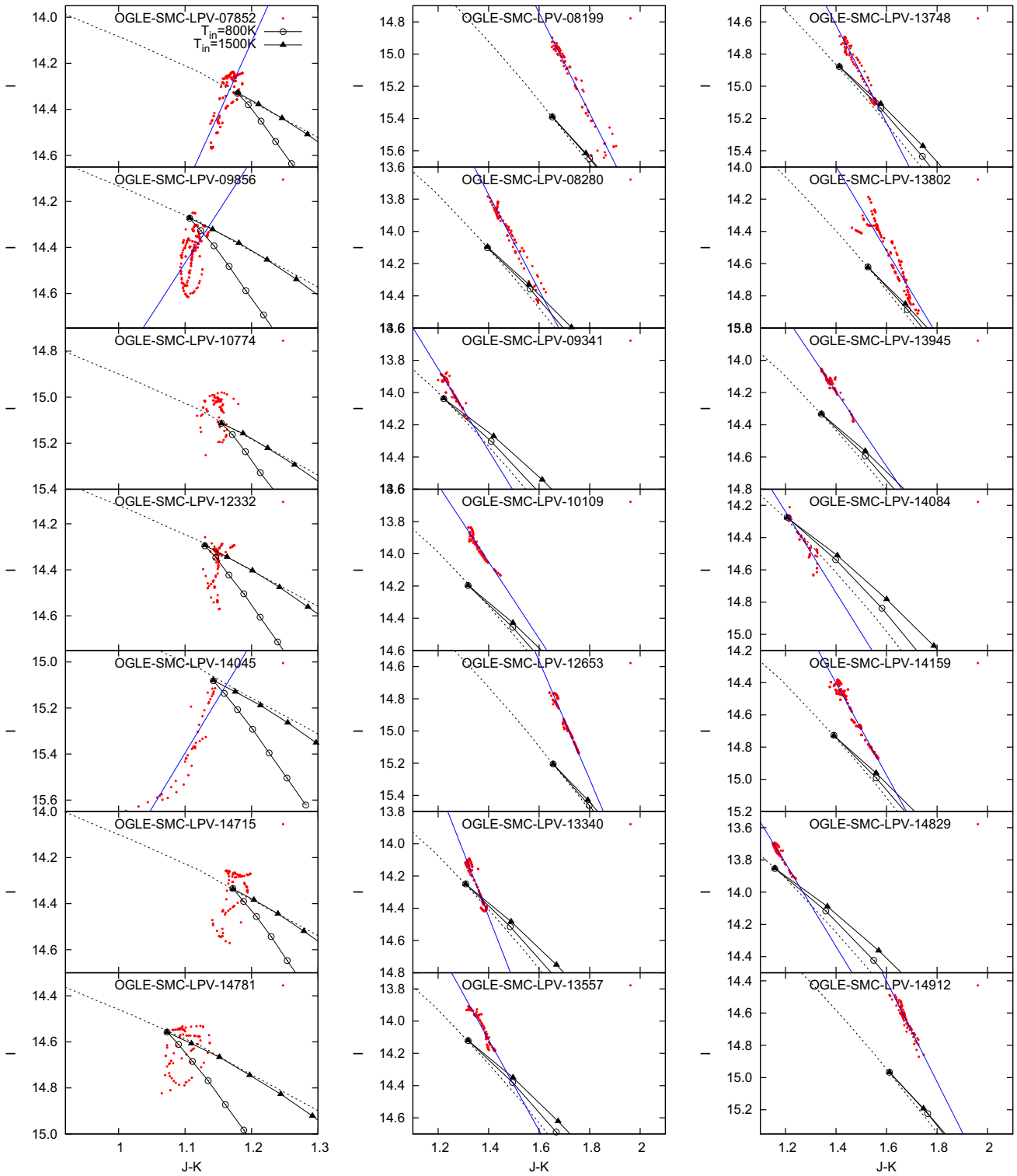

Figure 5. The same as Fig. 3 but using the $J - K_s$ colour rather than $I - J$.

where Ψ is the dust-to-gas mass ratio, Q_λ is the absorption efficiency of the grain at wavelength λ, a is the grain radius and ρ_g is the grain density.

We have used the DUSTY code (Ivezić et al. 1999) to examine the effect of a spherical dust shell on the broad-band colours of LSP stars. DUSTY computes the spectral energy distribution (SED) of a dust-enshrouded LSP star for one given configuration of the dust shell. From equation (1), we can see that the innermost dust shell plays the most important role for dust extinction when multiple dust shells of similar origin exist. In our model we only consider the innermost dust shell.

The first input parameter for DUSTY which we consider is the dust shell thickness. AGB stars are well-known mass-losing stars in which the terminal velocity of the mass flow is ∼10–20 km s^{-1}

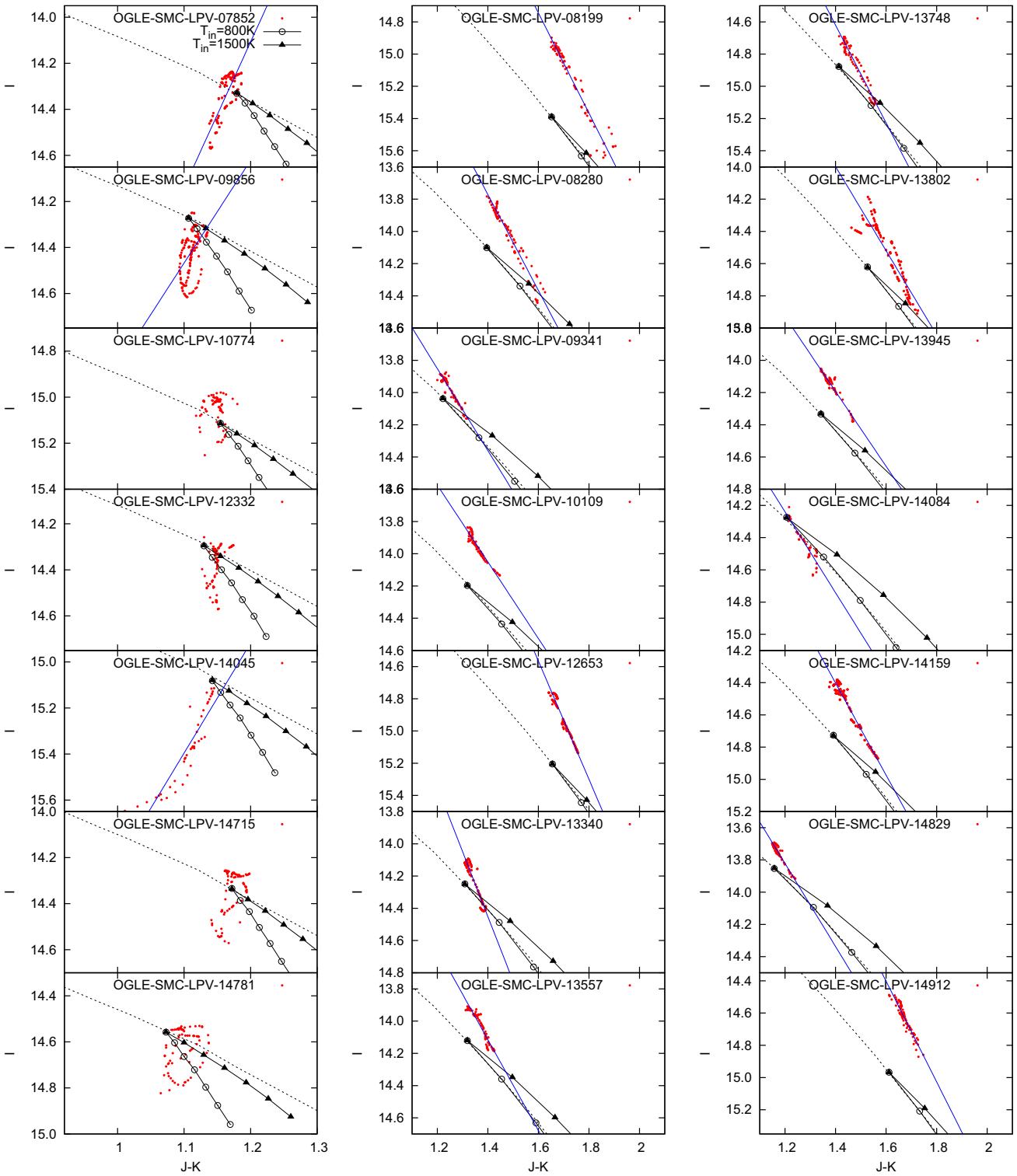

Figure 6. The same as Fig. 4 but using the $J - K_s$ colour rather than $I - J$.

(Decin et al. 2007; De Beck et al. 2010; Lombaert et al. 2013). On the other hand, RCB stars are similarly luminous evolved stars which eject mass semiperiodically in random directions (Clayton 1996). The large-amplitude variability of these stars is due to dust absorption by those ejected dust clouds which lie in the line of sight to the star. Observationally, the ejection velocity of the clouds is ~200–250 km s^{-1} (Feast 1975; Clayton 1996; Feast 1990). In view of these velocity estimates, and since we do not know what causes dust shell ejections in LSP stars, we considered two values for the wind velocity v of 15 and 220 km s^{-1}, and the velocity is assumed to be constant with radius. We assume that dust is ejected for a time interval equal to half the length of the LSP so the shell thickness is

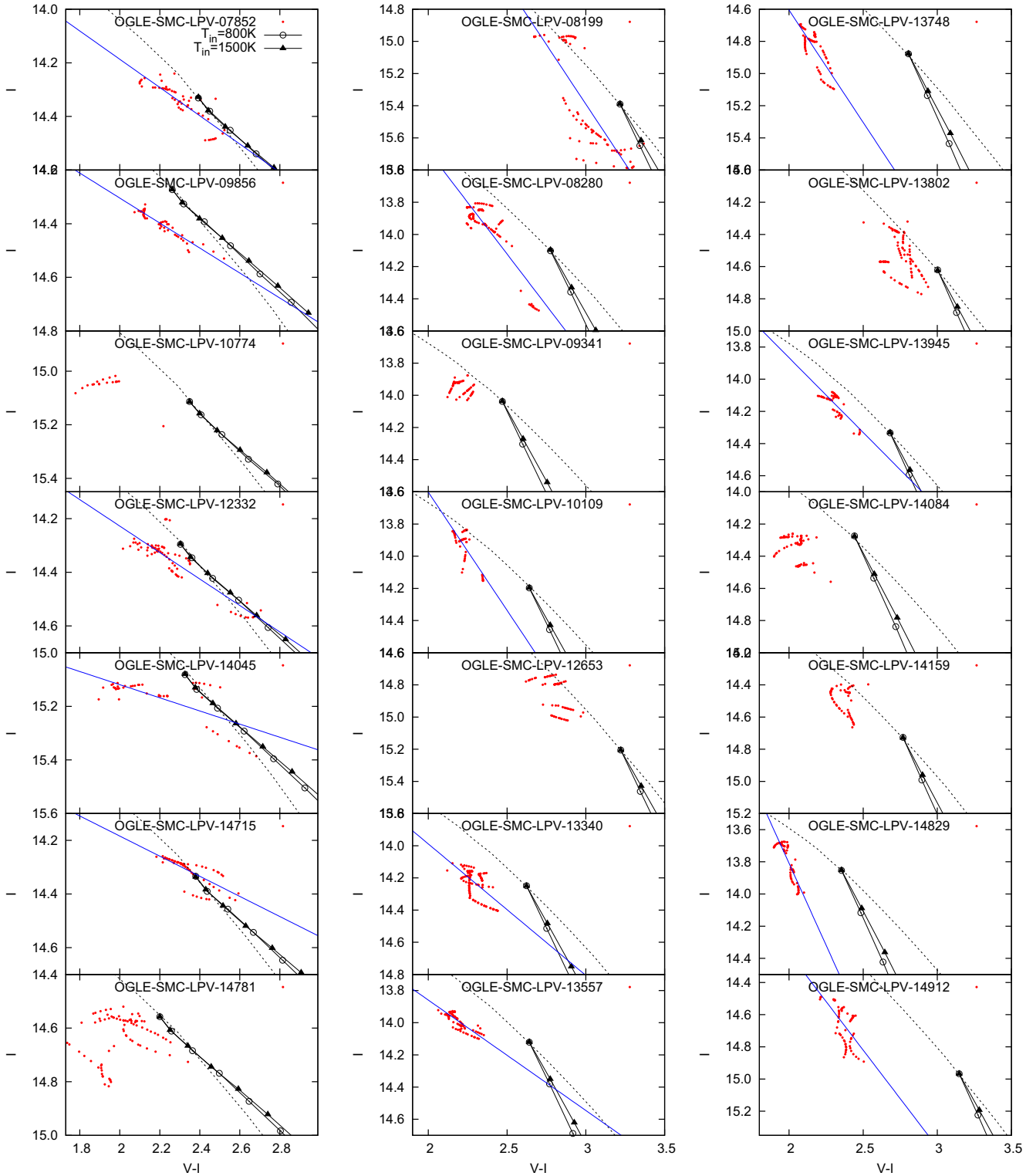

Figure 7. The same as Fig. 3 but using the $V - I$ colour rather than $I - J$.

$vP/2$, where P is the length of the LSP. Our models are thus made with two values for the shell thickness.

The second input parameter we require for DUSTY is the temperature $T_{\rm in}$ at the inner edge of the dust shell. We assume $T_{\rm in}$ is the dust condensation temperature. The dust condensation temperature is commonly assumed to lie in the range of 800–1500 K (e.g. van Loon et al. 2005; Cassarà et al. 2013) and in our models we consider $T_{\rm in}$ values of 800 and 1500 K. We note that $T_{\rm in}$ determines the inner radius of the dust shell.

The third input parameter for DUSTY is the grain type. The assumed chemical composition of the grains is different for models of oxygen-rich stars and carbon stars. van Loon et al. (2005) used DUSTY

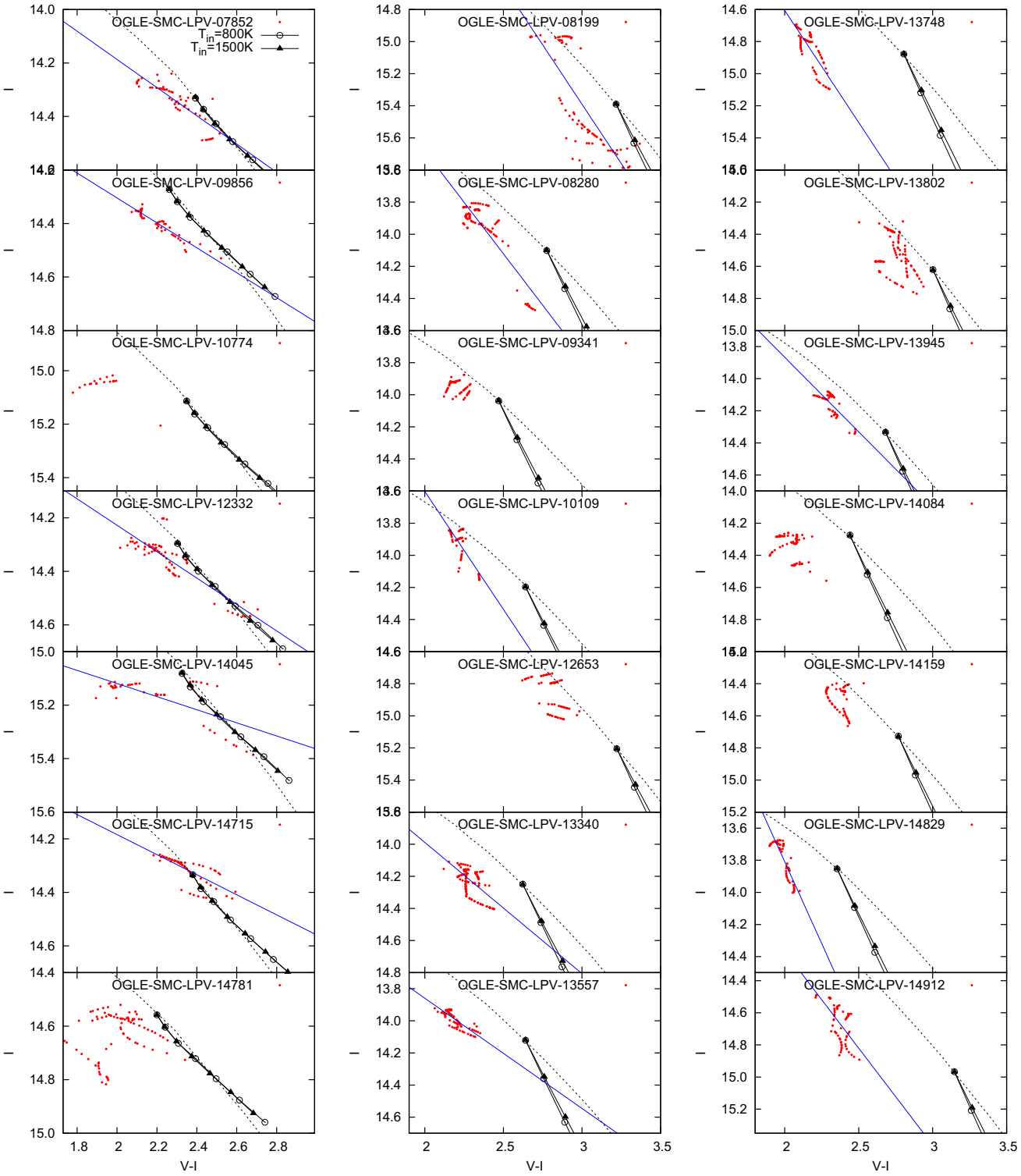

Figure 8. The same as Fig. 4 but using the $V - I$ colour rather than $I - J$.

to empirically determine possible grain types for oxygen-rich and carbon AGB stars in the LMC by requiring an acceptable fit to the SED of the observed stars. We use the grain chemical composition that they adopted. For carbon stars, we use dust grains of 50 per cent amorphous carbon from Hanner (1988), 40 per cent graphite from Draine & Lee (1984) and 10 per cent SiC from Pègouriè (1988) and for oxygen-rich stars, we use the astronomical silicates of Draine & Lee (1984).

The stellar luminosity L and the effective temperature $T_{\rm eff}$ of our LSP stars are also required as input to DUSTY. These were computed from the J and $K_{\rm s}$ magnitudes at maximum light, when circumstellar extinction is minimum. The $T_{\rm eff}$ values for the observed stars

Table 3. Dust composition.

Sp. type	Model name	Composition
O-rich star	model 0	100 per cent [1]astronomical silicate
	model 1	100 per cent [2]warm O-deficient silicate
	model 2	100 per cent [3]FeO
	model 3	100 per cent [4]glassy olivine
C-rich star	model 0	50 per cent [5]amorphous carbon, 40 per cent [1]graphite, 10 per cent [6]α-SiC
	model 1	100 per cent [1]graphite
	model 2	100 per cent [5]amorphous carbon
	model 3	100 per cent [6]α-SiC

Note. [1]Draine & Lee (1984), [2]Ossenkopf, Henning & Mathis (1992), [3]Henning et al. (1995), [4]Dorschner et al. (1995), [5]Hanner (1988), [6]Pègouriè (1988).

were estimated from the $J - K_s$ colour at maximum light using the formula given in Bessell et al. (1983). We also used $J - K_s$ to calculate a blackbody temperature T_{BB} for the central star at maximum. Luminosities were computed using a bolometric correction BC_K to the K_s magnitude. For oxygen-rich stars, we adopted the formula $BC_K = 0.60 + 2.56(J - K) - 0.67(J - K)^2$ given by Kerschbaum, Lebzelter & Mekul (2010) and for carbon stars we adopt the formula $BC_K = 1.70 + 1.35(J - K) - 0.30(J - K)^2$ given by Bessell & Wood (1984). To estimate the absolute bolometric magnitude, we used the distance modulus of 18.93 given to the SMC by Keller & Wood (2006). The derived values for L, T_{BB} and T_{eff} are listed in Table 1. When using DUSTY, we assumed that the central star emits a blackbody spectrum of temperature T_{BB}. We are only interested in *changes* in magnitudes and colours, rather than the absolute values of the colours and magnitudes, and the blackbody assumption will have only an insignificant effect on these changes.

The final input parameter to DUSTY is the optical depth τ_V in the V band. The output from DUSTY is the SED of the central star extincted by a shell of visible optical depth τ_V. Unless there is significant emission from the dust shell in each band under consideration, for a given value of τ_V the extinction of the central star in each band is essentially independent of the details of the shell radius or thickness.

4.2 Comparison of the dust model with observations

4.2.1 The variation of I with I − J

In general, the I light curves are the best sampled of the light curves in the different filters, the J, H and K light curves are the next best sampled and the V light curves are mostly only sparsely sampled. Thus when comparing observations against models in magnitude–colour plots, we use I as the magnitude and a colour involving I and another magnitude. The other magnitude should be one of J, H or K because of the higher frequency of observation compared to V. Ideally, $I - K$ would be best because of the large wavelength range spanned by this colour, but as we will show below, the K band in O-rich stars is contaminated by variable H_2O absorption, as is the H band, so we use $I - J$ as the colour in our first comparison of observations and models.

In Figs 3 and 4 we show the I magnitude plotted against the $I - J$ colour for the observed samples of oxygen-rich and carbon stars. Fig. 3 displays models with a shell expansion velocity of 15 km s^{-1} (thin shell) while Fig. 4 displays models with a shell expansion velocity of 220 km s^{-1} (thick shell). Note that it is not the absolute values of points in the diagrams that is important, it is the slope of the line representing the variation of I with $I - J$ that matters. If the LSP variations are caused by variable amounts of circumstellar dust alone, then the slope will depend almost entirely on the dust properties and not on the spectrum of the central star. The central star, which in these models we assume to emit as a blackbody with the L and T_{BB} given in Table 1, determines the position of the model in Figs 3 and 4 when there is no circumstellar extinction.

First, we make some comments on the models. In both Figs 3 and 4, the two model lines differ slightly due to re-emission from the dust shell at J and to a lesser extent I. Comparing Fig. 3 with Fig. 4, corresponding to models with different dust shell thickness, we see that there is a slightly faster increase in $I - J$ with I for the thinner shell of Fig. 3, especially for the hotter inner dust shell temperature of 1500 K. The reason for this is that for the thinner dust shell there is more emission at J. Also, for a given optical depth τ_V to the centre of the disc of the observed star, the total extinction averaged over the stellar disc is slightly greater for the thinner shell in Fig. 3 than for the thicker shell in Fig. 4 (the lines in Fig. 3 are longer than in Fig. 4). This is because the extinction near the limb of the disc is smaller relative to the extinction at the centre of the disc for a thicker shell.

The observed variation of I with $I - J$ associated with the LSP (red points) is generally consistent with the slope of one of the model lines in Figs 3 or 4. This indicates that the variation of I and J due to an LSP could be explained by variable dust absorption alone.

4.2.2 The variation of I with J − K_s

Figs 5 and 6 show the variation of I with $J - K_s$. As one can easily see, the observational variations due to the LSPs are inconsistent with the model variations in all cases. Most importantly, for the O-rich stars, the observed $J - K_s$ colour tends to get *bluer as the star gets fainter in* I. There is no way that such variations can be the result of variable amounts of dust extinction only.

The most probable explanation for the variation of $J - K_s$ in O-rich LSP stars is strong H_2O absorption in K_s band. Significant broad H_2O band absorption is found between about 1.4 and 1.9 μm on the edges of the H and K_s filter bandpasses. In non-variable stars, this absorption is seen from about M6 III to later spectral type in M giants (e.g. Tsuji 2000; Rayner, Cushing & Vacca 2009). Strong water absorption in the H and K bands is also commonly seen in large amplitude pulsating red giants (Mira variables; e.g. Johnson & Méndez 1970). The reason for this absorption is the existence of a relatively dense shell with a temperature of about 1800 K elevated above the photosphere by shock waves associated with the pulsation (Ireland, Scholz & Wood 2011). Using the models atmosphere results of Houdashelt et al. (2000), we find that the $V - I$ colours of the stars we are examining here yield T_{eff} ∼3400–3600 K, corresponding to spectral types M3–M5. Due to these relatively early M spectral types, the results noted above mean that strong water absorption in the K_s band cannot occur in a hydrostatic atmosphere. The elevation of a shell of mass above the photosphere is required to produce strong water absorption, as in the case of Mira variables. We suggest that this shell elevation, which may also lead to dust formation, occurs at the beginning of the luminosity declines associated with the LSPs, leading to the formation of increasing H_2O absorption in the K_s band and blueing of the $J - K_s$ colour.

This result is a second piece of observational evidence for the existence of a disturbance above the photosphere caused by the LSP. Wood et al. (2004) found variable Hα absorption in stars with LSPs which they attribute to a chromosphere of variable strength, with

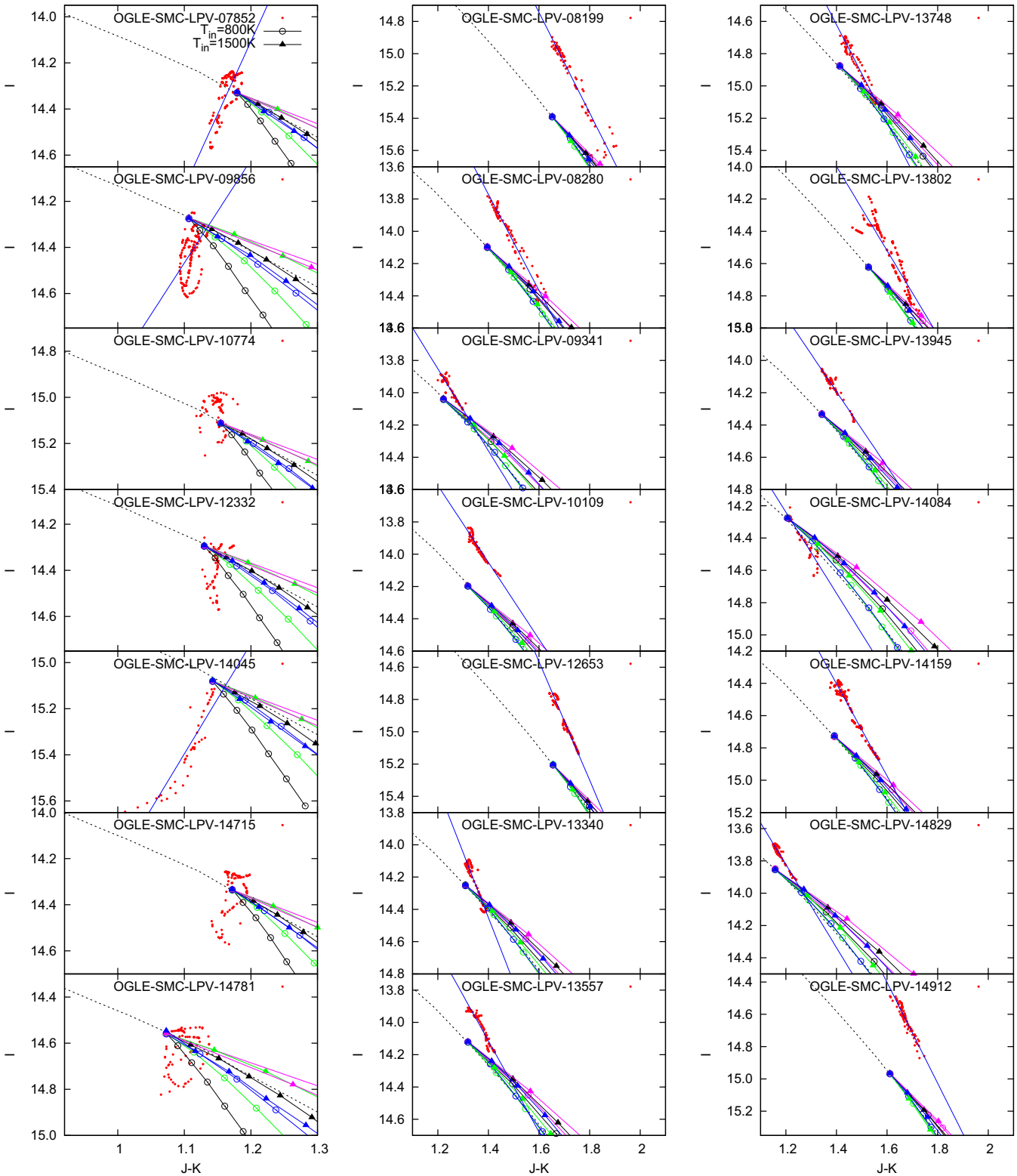

Figure 9. The same as Fig. 5 but including different dust compositions. For both oxygen-rich and carbon stars, the black solid lines with open circles and filled triangles correspond to the original dust compositions (model 0 in Table 3), while the green, magenta and blue colours correspond to models 1, 2 and 3, respectively.

Table 4. Spot temperatures and the spot sizes.

Sp. type	Temperature ratio	Spot radius(°)	Model
O-rich star	0.533	35	cool
	0.833	45	warm
	0.913	90	hemisphere
C-rich star	0.533	40	cool
	0.833	50	warm
	0.888	90	hemisphere

Note. Spot radius is defined as the angle when viewed from the stellar centre.

the strongest Hα absorption near maximum light. Combined with the results above for the H_2O absorption layer, we have a picture whereby matter is ejected above the photosphere beginning near the luminosity decline of the LSP forming a relatively dense shell of temperature ∼1800 K. As the LSP cycle progresses, this shell appears to be slowly heated by non-thermal processes to ∼8000 K giving rise to a chromosphere which is then displaced by the next ejected shell containing H_2O.

Turning to the carbon stars, we see that they do get redder as they get fainter in I but in all cases they clearly do not redden as much as predicted by the models. To bring the observed variation in $J - K_s$ with decline in I into agreement with the models, while keeping the variation of $I - J$ with I in agreement with the models, would require a strange dust opacity with a large bump in the K_s band. We do not know of any dust composition that could produce such a bump (see Section 4.2.4 for a discussion of the effect of different grain opacities).

We note that ejected clouds covering only part of the stellar surface rather than the complete surface as for spherical shells cannot explain the observed variation in $J - K_s$ with declining I. For all but very large optical depths, the $J - K_s$ colour in a cloud model increases slightly faster with decline in I than for a spherical shell model, whereas the observations require a slower increase in $J - K_s$ colour. Also, given that the variation of the observed $I - J$ colour with decline in I agrees with the spherical shell models, a cloud model will not agree with the observations (the $V - I$ colour in the cloud model increases more slowly with decline in I than in the spherical shell model).

In summary, our conclusion from examining the variations of LSP stars in the (I, $J - K$) plane is that, for both O-rich and C-rich stars, a model involving only variable dust extinction is not viable as an explanation for LSP behaviour.

4.2.3 The variation of I with V − I

Although the V observations are not as frequent as observations in other bands, we show the variation of I with $V - I$ for completeness in Figs 7 and 8. For both the V and I bands, re-emission of light absorbed by the shell is weak so the model lines corresponding to the two inner shell temperatures of 800 and 1500 K are close together in both figures.

For most O-rich stars, the observed $V - I$ tend to increase slightly more rapidly with declining I than in the models. For most C-rich stars, the observed and model variations have consistent slopes although for OGLE-SMC-LPV-13557 and OGLE-SMC-LPV-13945 the slopes are different. Overall, the agreement between the observations and dust model predictions is not good in the (I, $V - I$) plane but the results are not definitive.

4.2.4 Testing different dust grains

Different dust grains have different absorption and scattering coefficients. Thus we tried changing the dust grain composition to see if this would give agreement between the light variations in the dust shell model and the observed light variations, especially in the I and $J - K_s$ plane for the carbon stars. We examined four dust grain types available in DUSTY (see Table 3) for oxygen-rich stars and for carbon stars, including the grain types we used in Section 4.1. The thin dust shell model with an expansion velocity of 15 km s^{-1} was adopted.

Fig. 9 shows comparisons of observed variations in the I and $J - K_s$ diagram with dust shell models for the different grain types. The model slopes for oxygen-rich stars can be changed appreciably by different dust grains but none of the models reproduce the observed slopes. In particular, none of the models can explain the observation that the $J - K_s$ colour get bluer as the star gets fainter in I. Turning to the carbon stars in Fig. 9, we see that changing the grain type in the models changes the slope of the variations but again none of the adopted grain types can consistently reproduce the observed slope. These results strengthen the finding of Section 4.2.2 that dust shell models cannot by themselves explain the broad-band light and colour variations in LSP stars.

4.3 The dark spot model

Another possible explanation of the LSP phenomenon is a dark spot on a rotating AGB star. Soszyński & Udalski (2014) noted that the observed light curves of LSP stars are similar to those of the known spotted stars. Moreover, the V to I amplitude ratios of LSP stars and known spotted stars are similar and they are different from the ratios seen in the ellipsoidal binaries of sequence E which lie near the LSP stars in period–luminosity plots. Here we test a simple rotating dark spot model for LSP stars using the latest version of the Wilson–Devinney code (Wilson & Devinney 1971) which has the ability to simulate the light curve of a spotted star in a binary system. Since our aim is to examine the light and colour variations due to the appearance of a dark spot on a red giant, our binary systems consist of a rotating red giant star with a circular isothermal spot and a very faint orbiting companion which cannot be seen. Hence, we obtain the light and colour variations due to only the dark spot on the rotating red giant. For the red giant star, we assume a mass of ∼1.0 $M_\odot$ and a radius of ∼170 $R_\odot$, which gives a surface gravity log g [cgs] of −0.02. A metallicity, log [Fe/H] = −1.0 and a gravity-darkening coefficient, $g_1 = 0.32$ (Lucy 1967) are used. For the calculation of oxygen-rich stars, we use the model stellar atmospheres of van Hamme & Wilson (2003) while for carbon stars, a blackbody is used. We note that the model atmospheres do not take into account the effect of the absorption due to H_2O molecules.

The amplitudes of the light variations due to the presence of spots are determined by the spot sizes and the temperature differences between the spots and the normal stellar surface. The temperatures of spots on AGB stars are not known well. For the spot temperature, we follow the work of Soker & Clayton (1999). They initially adopted the solar value of $\frac{2}{3}$ for the ratio of spot to normal photospheric temperature. For an assumed photospheric temperature of 3000 K, the spot temperature would then be 2000 K. Soker & Clayton (1999) then considered a range of spot temperatures from 1600 K (cool spot) and 2500 K (warm spot) corresponding to a ratio of spot to normal photospheric temperature of 0.533 and 0.833, respectively. To cover a range of spot temperatures, we also make models with these two temperature ratios. We use these models to simulate each

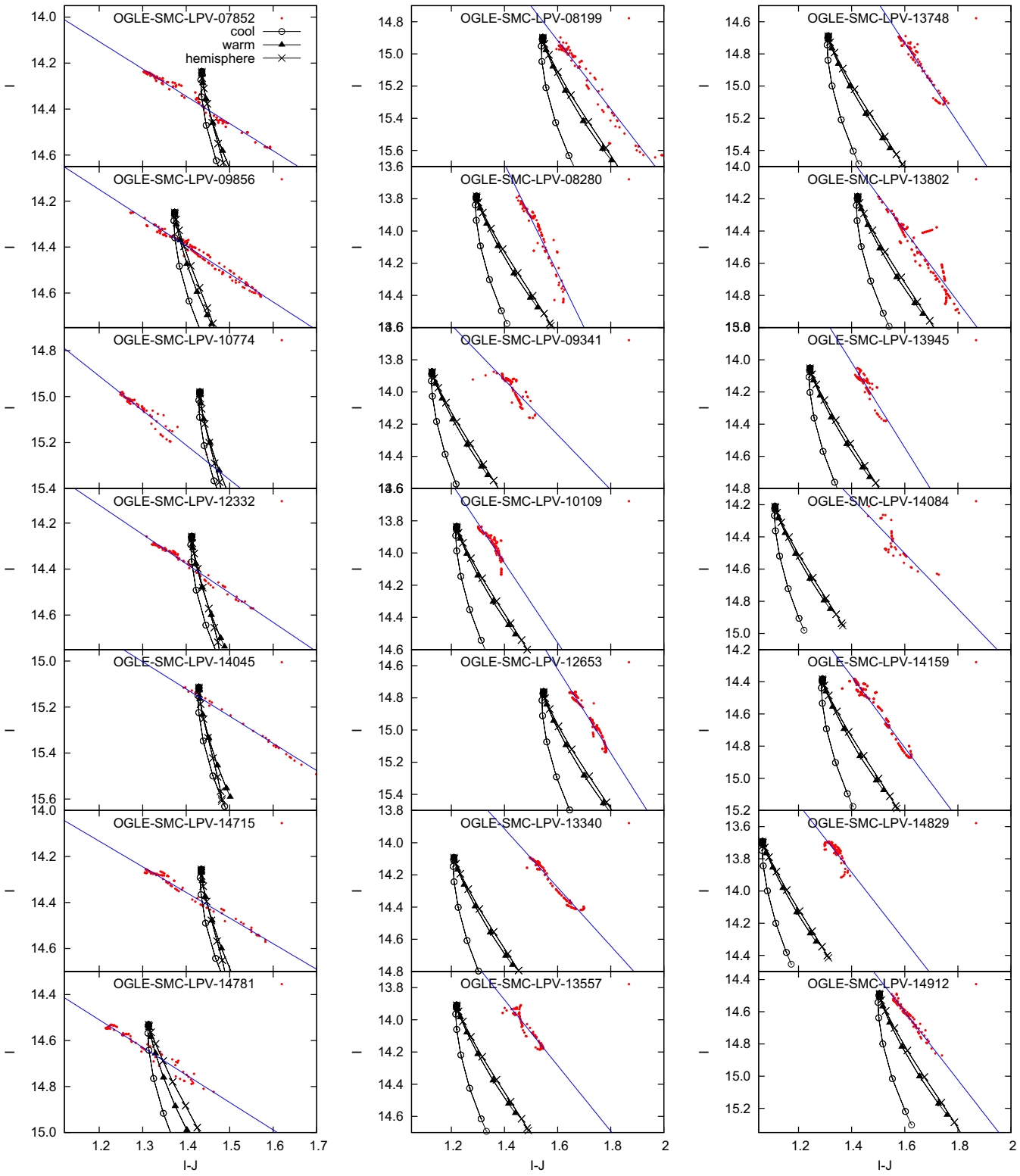

Figure 10. Comparisons of observations with dark spot models in the $(I, I-J)$ plane. The 7 panels of the left-hand column show oxygen-rich stars and the 14 panels of middle and right-hand columns show carbon stars. Red points and blue lines represent observations, as in Fig. 3. The black lines with open circles and the lines with filled triangles show the magnitude and colour variations for models with cool and warm spot temperatures, respectively, while the lines with crosses are for models with a hemisphere spot.

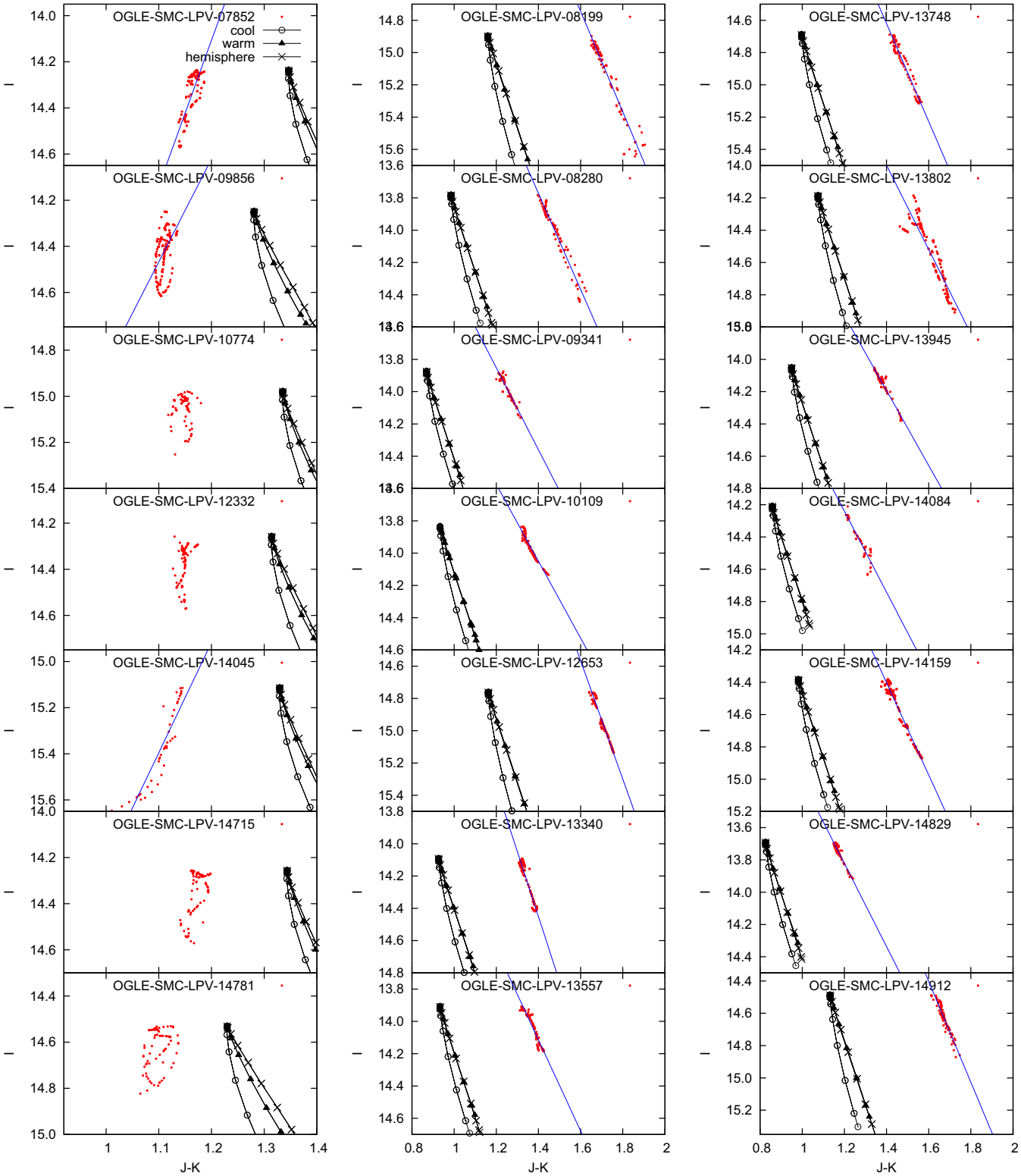

Figure 11. The same as Fig. 10 but using the $J - K_s$ colour rather than $I - J$.

of the stars in Table 1 and we use the effective temperatures $T_{\rm eff}$ in Table 1 as the temperature of the normal photospheric regions.

The spot sizes for the two temperature cases are fixed by requiring that the amplitude in the I band is similar to the observed largest amplitudes, which are ∼0.5 mag for the oxygen-rich stars and ∼0.7 mag for the carbon stars. Table 4 gives the parameters of our spot models. It has been assumed that the inclination of the model rotation axis is 90 deg to the line of sight and the centre of the spot is on the equator of the star.

The spot model also effectively simulates light variations caused by the giant convective cells which were proposed by Stothers (2010) to explain LSPs in AGB stars. In this model, the light

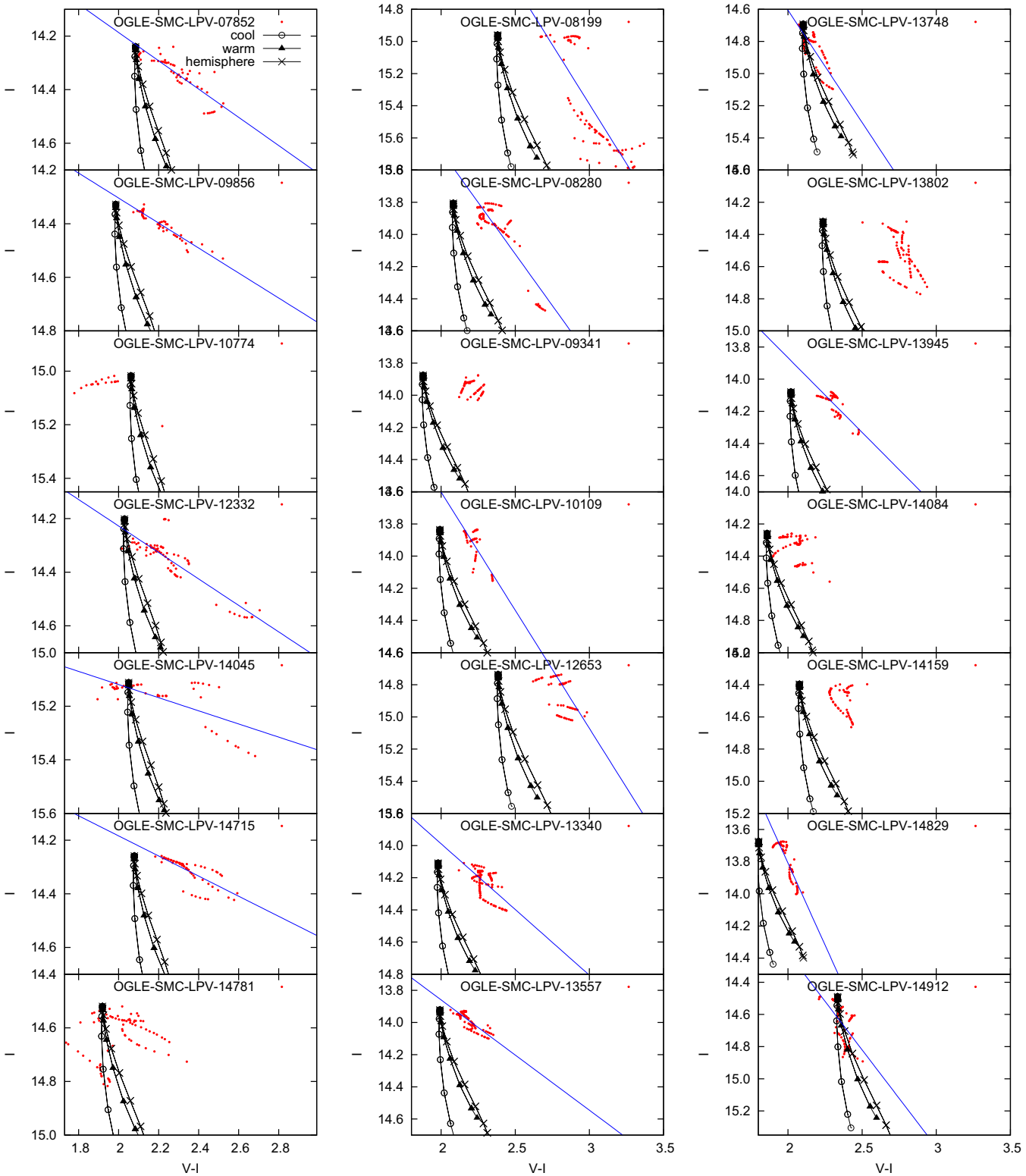

Figure 12. The same as Fig. 10 but using the $V - I$ colour rather than $I - J$.

variations are caused by the turnover of cooler and hotter giant convective cells at the stellar surface. To simulate this situation, we examine a model where the rotating dark spot covers a full hemisphere of the star (hereinafter, the hemisphere model). To reproduce the observed largest amplitudes in I band, we use the temperature ratios of the spot area to the normal area given by Table 4. As in the case of the other spot models, we use the effective temperatures $T_{\rm eff}$ given in Table 1 for the temperature of the normal photospheric regions in both oxygen-rich and carbon stars.

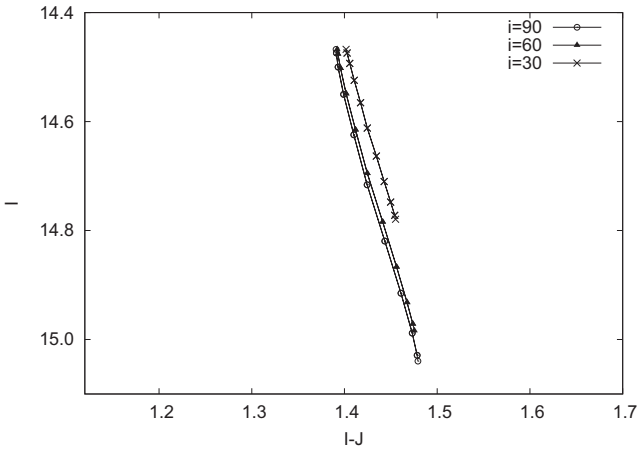

Figure 13. The variation of I with $I - J$ in hemisphere spot models for oxygen-rich stars when different inclination angles for the rotation axis are assumed.

Table 5. $\Delta T_{\rm eff}$ and $\tau_{\rm V,\,0}$ for models.

Sp. type	$T_{\rm eff,\,0}$(K)	$\Delta T_{\rm eff}$(K)	$\tau_{\rm V,\,0}$	Model
O-rich star	2800	100	1	model 0
	2800	50	2	model 1
C-rich star	2500	100	0.5	model 2
	2500	50	1	model 3

4.4 Comparison of the spot model with observations

4.4.1 The variation of I with colours

In Figs 10, 11 and 12 we show the I magnitude plotted against the colours $I - J$, $J - K_{\rm s}$ and $V - I$, respectively, for the observed samples of oxygen-rich and carbon stars. The magnitudes of models at the maximum light, which corresponds to when there is no visible spot, are adjusted in the plots to the magnitudes at the observed maximum light for each star.

As with our comparison of dust shell models with observations, we test the spot models by looking for differences in the slopes in (I,colour) diagrams of model lines and observational variations. Models with different ratios of the spot to normal photospheric temperature show different slopes. The models with higher spot temperature (i.e. larger temperature ratio) show shallower slopes.

For carbon stars, the slope of the line representing the observations generally shows a good agreement with the model lines in each of Figs 10, 11 and 12 (two exceptions are OGLE-SMC-LPV-13557 and OGLE-SMC-LPV-13945 in Fig. 12 which show disagreement with their models). According to the figures, the models with hotter spots (temperature ratio 0.833) and the hemisphere models (which also have a temperature ratio of 0.888) fit the models better in each of the (I, $I - J$), (I, $J - K_{\rm s}$) and (I, $V - I$) diagrams. If sequence D light variations are due to rotating spots, these results suggest that the spot temperatures in carbon stars should be roughly 2500 K.

In distinct contrast to the carbon stars, the oxygen-rich star variations do not agree with model variations in any of the (I, $I - J$), (I, $J - K_{\rm s}$) or (I, $V - I$) diagrams. Although agreement would not be expected in the (I, $J - K_{\rm s}$) plane where the observations are affected by absorptions due to H_2O molecules, the bad disagreement in the (I, $I - J$) and (I, $V - I$) diagrams indicates that spot models cannot explain the light and colour variations due to the LSP phenomenon in oxygen-rich stars. Since the LSPs of both oxygen-rich stars and carbon stars should have the same origin, the failure of the spot models to reproduce the observations in oxygen-rich stars means that spots are not a reasonable explanation for LSPs in sequence D stars. This result agrees with the conclusion of Olivier & Wood (2003) that the rotation periods of LSP stars are too long for a spotted star model to explain LSP variations.

4.4.2 The effect on spot models of the inclination of the rotation axis and the spot latitude

The models above were made assuming spots on the equator of a rotating star whose rotation axis is perpendicular to the line of sight. Changing the latitude of a spot will reduce its apparent area and hence the amplitude of the light variation it will cause. However, the slope of the locus of colour–magnitude variation should be unchanged since the reduction in apparent area also occurs as a spot on the equator rotates towards the limb of the star (the very minor effect of limb darkening will produce very small differences between the two cases). The same argument applies in the case of a star with a tilted rotation axis. We thus expect the results of the previous section to apply regardless of the inclination of the rotation axis and the latitude of the spots. As a test calculation, we examined the change in the I and $I - J$ magnitudes for a star with the rotation axis tilted at 30, 60 and 90 deg. The results are shown in Fig. 13. It can be seen that the slope of the variation is the same in all cases.

4.5 A combined dust and dark spot model

In Section 4.2 the possibility that a dust shell model alone could explain the LSP phenomenon was examined and rejected. Similarly, in Section 4.4 a rotating spotted star model was examined and rejected. Here we examine the possibility that a combination of a rotating spotted star and dust absorption at certain phases of the rotation could cause the observed behaviour of stars with LSPs.

In this combined model, the effective temperature of the central star is assumed to vary sinusoidally to simulate a rotating spotted star and the optical depth of the dust shell is assumed to vary sinusoidally to simulate periodic dust absorption. The following equations are used:

$$T_{\rm eff}(\phi) = T_{\rm eff,0} + \Delta T_{\rm eff} \sin(2\pi\phi + \beta) \tag{2}$$

$$\tau_{\rm V}(\phi) = \tau_{\rm V,0} \sin(\pi\phi), \tag{3}$$

where $\Delta T_{\rm eff}$ and $\tau_{\rm V,\,0}$ are the amplitudes of variation of the effective temperature and the optical depth in V of the dust shell, respectively. $T_{\rm eff,\,0}$ is the average effective temperature. As a direct consequence of these equations, the central star luminosity is given by

$$L(\phi) = \frac{T_{\rm eff}^4(\phi)}{T_{\rm eff,0}^4} L_0, \tag{4}$$

where L_0 is the average luminosity. The fluxes emitted by the central star in the various photometric bands were obtained assuming the central star was a blackbody. The dust absorption in photometric bands other than V was obtained using DUSTY. The dust compositions used in Section 4.1 for oxygen-rich and carbon-rich stars was adopted and the shell outer radius was set to 1.5 times the inner radius, which roughly corresponds to the models described above with an expansion velocity of 15 km s^{-1}. The inner dust shell temperature was set to 800 K.

In the combined model, ϕ varies from 0 to 1 as the spotted star makes one complete rotation. The phase shift β between the rotation

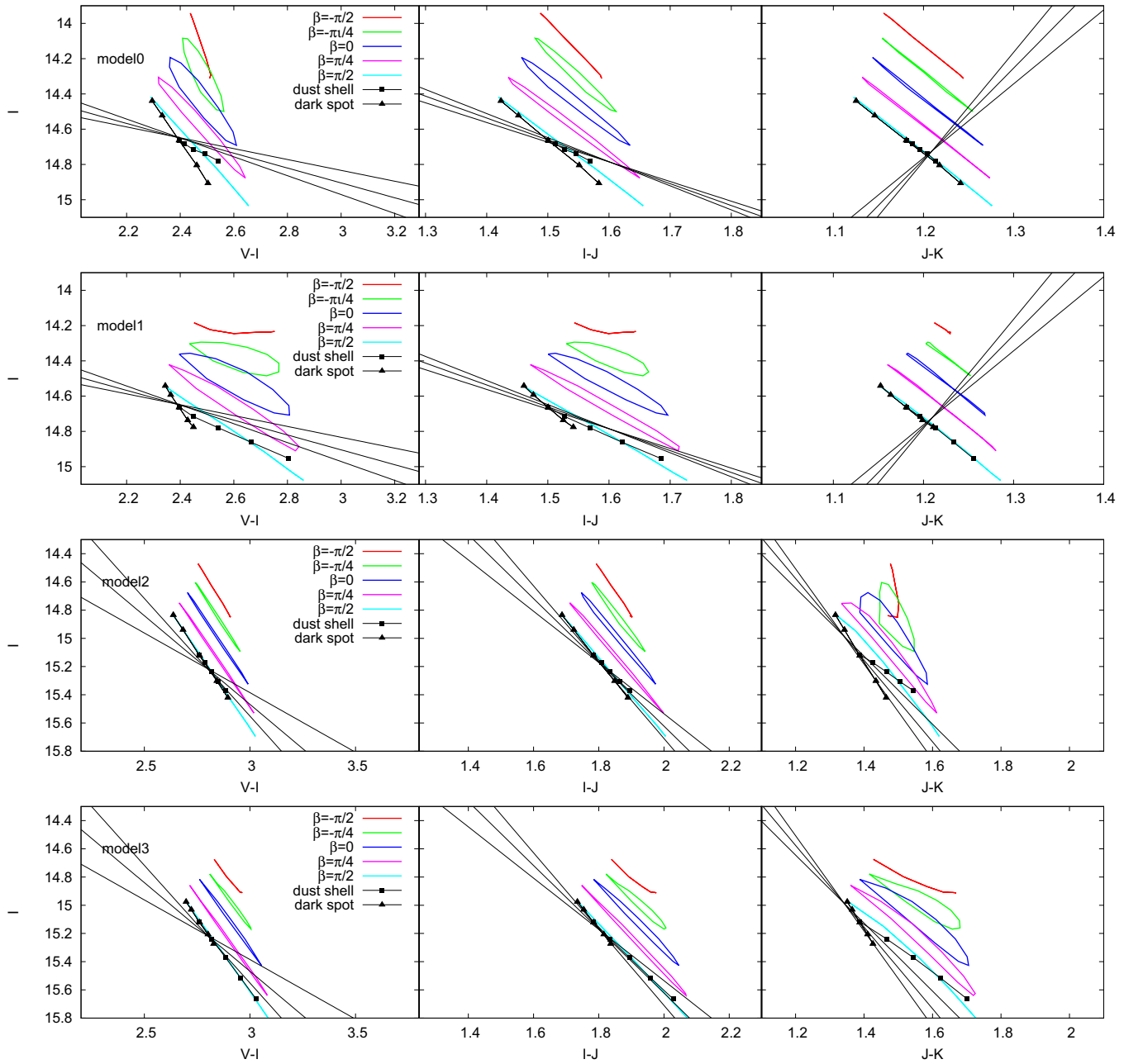

Figure 14. The variations of I with $V-I$, $I-J$ and $J-K$ for the models listed in Table 5. Models for oxygen-rich stars are shown in the upper two panels and models for carbon-rich stars are shown in the lower two panels. Solid lines with filled squares represent the dust shell model alone while solid lines with filled triangles represent the dark spot model alone. The combined dust and rotating spotted star models are shown as coloured lines with the colour indicating the phase lags β. Note that the coloured lines have been arbitrarily shifted in I to prevent confusing overlap since it is only the slope of the lines that is of interest. The slopes of the three solid black lines in each diagram represent the observed variations. The central line corresponds to the mean value of the observed line slope for stars with a relative error in the slope of less than 0.2 and the outer lines vary from the mean slope by 1σ.

phase and dust absorption phase has been introduced to allow for dust absorption at different possible rotation phases. Since we do not know how dust absorption might be linked to the rotation phase, models were made with different values for β. Note that the dust absorption goes through one maximum as the star makes a full rotation.

Table 5 gives the parameters considered for the models described here. Two values of $\Delta T_{\rm eff}$, 50 and 100 K, were used for both oxygen-rich and carbon-rich stars. The values of $\tau_{\rm V,\,0}$ were adjusted so that the variations in magnitude caused by dust dominated for the models with $\Delta T_{\rm eff} = 50$ K while the variations in magnitude caused by $T_{\rm eff}$ variations dominated when $\Delta T_{\rm eff} = 100$ K.

Fig. 14 shows the I magnitude plotted against $V-I$, $I-J$ and $J-K$ for the various models computed here. In general, the slopes of the variations in the (I,colour) diagrams for the combined models lie between the slopes for pure dust absorption and pure $T_{\rm eff}$ variations (spot model). The combined models do not generally represent an improvement over the pure dust or spot models. In particular, they cannot explain the observation that $J-K$ in oxygen-rich stars get bluer as the star dims.

5 SUMMARY

We have examined broad-band observations of samples of oxygen-rich and carbon stars in the SMC which exhibit LSP light variations. The observations are in the *VIJHK*$_s$ bands and they were obtained by the OGLE project and by the SIRIUS camera of the IRSF 1.4 m telescope.

The J and K_s observations of oxygen-rich stars reveal a significant new feature of LSP light variations. As light declines, the $J - K_s$ colour barely changes or sometimes gets bluer. We interpret this as indicating that cool gas containing a significant amount of H_2O is levitated above the photosphere of LSP stars at the beginning of light decline. Absorption of light in the K_s band by H_2O forces the $J - K_s$ colour to remain constant or to get bluer during light decline. The levitation of matter above the photosphere found here, along with the discovery of the development of a warm chromosphere during rising light by Wood et al. (2004), provides strong evidence that the LSP phenomenon is associated with mass ejection from the photosphere of red giant stars.

We examined two possible models for the explanation of the LSP phenomenon by comparing these models with broad-band observations of both oxygen-rich and carbon stars. The first model assumes LSP light variations are due to dust absorption by ejected dust shells while the second model assumes a rotating star with a dark spot.

In the dust shell ejection model for LSP stars, it was found that dust absorption by the ejected mass shell could not explain the observed variations in the (I, $J - K_s$) or (I, $V - I$) diagrams for either oxygen-rich or carbon stars. In oxygen-rich stars, the models fail to reproduce the variations in the (I, $J - K_s$) because the models only include variable dust absorption and not the variable H_2O absorption noted above. The failure of the dust shell models to reproduce the observed variations in the (I, $V - I$) diagram for either oxygen-rich or carbon stars, and the failure to reproduce the observed variations in the (I, $J - K_s$) diagram for carbon stars, suggests that dust absorption in ejected mass shells is not the cause of LSP light variations.

The LSP model involving a rotating, spotted star was not able to reproduce the observed variations in oxygen-rich stars in either the (I, $I - J$) or (I, $V - I$) diagrams (or the I, $J - K_s$ diagram, but here the $J - K_s$ colour is affected by H_2O absorption that is not included in the models). We thus conclude that the rotating, spotted star model is not the explanation for LSP light variations either. This result strengthens the conclusion of Olivier & Wood (2003) that the rotation periods of LSP stars are too long for a spotted star model to explain LSP variations. A simple combined dust and spotted star model was no better at explaining the observed magnitude–colour variations than the dust and spotted star models individually.

Our conclusion is that some process other than dust shell ejection or spot rotation lies behind the light variations seen in stars with LSPs. This unknown process seems to be responsible for the ejection of matter near the beginning of light decline. The ejected matter may be the origin of the excess mid-IR emission due to dust that is seen in stars with LSPs (Wood & Nicholls 2009).

ACKNOWLEDGEMENTS

MT gratefully acknowledges the hospitality and generous support of Professor Peter Wood and his colleagues during his long-term visit at the Australian National University where this work was written. He would also like to thank Professor Hideyuki Saio for useful discussions and help. The authors thank the referee for constructive comments. This research is supported by Brain Circulation Program (R2301) of the Ministry of Education, Science, Culture, and Sports in Japan. This research is partly supported by the Japan Society for the Promotion of Science through Grant- in-Aid for Scientific Research 26·5091.

REFERENCES

Bessell M. S., Wood P. R., 1984, PASP, 96, 247
Bessell M. S., Wood P. R., Evans T. L., 1983, MNRAS, 202, 59
Cassarà L. P., Piovan L., Weiss A., Salaris M., Chiosi C., 2013, MNRAS, 436, 2824
Clayton G. C., 1996, PASP, 108, 225
De Beck E., Decin L., de Koter A., Justtanont K., Verhoelst T., Kemper F., Menten K. M., 2010, A&A, 523, A18
Decin L., Hony S., de Koter A., Molenberghs G., Dehaes S., Markwick-Kemper F., 2007, A&A, 475, 233
Derekas A., Kiss L. L., Bedding T. R., Kjeldsen H., Lah P., Szabó G. M., 2006, ApJ, 650, L55
Dorschner J., Begemann B., Henning T., Jaeger C., Mutschke H., 1995, A&A, 300, 503
Draine B. T., Lee H. M., 1984, ApJ, 285, 89
Feast M. W., 1975, in Sherwood V. E., Plaut L., eds, Proc. IAU Symp. 67, Variable Stars and Stellar Evolution. Reidel, Dordrecht, p. 129
Feast M. W., 1990, in Cacciari C., Clementini G., eds, ASP Conf. Ser. Vol. 11, Confrontation Between Stellar Pulsation and Evolution., Astron. Soc. Pac., San Francisco, p. 538
Fraser O. J., Hawley S. L., Cook K. H., 2008, AJ, 136, 1242
Groenewegen M. A. T., de Jong T., 1993, A&A, 267, 410
Hanner M. S., 1988, NASA Conf. Publ., 3004, 22
Henning Th., Begemann B., Mutschke H., Dorschner J., 1995, A&AS, 112, 143
Hinkle K. H., Lebzelter T., Joyce R. R., Fekel F. C., 2002, AJ, 123, 1002
Höfner S., Feuchtinger M. U., Dorfi E. A., 1995, A&A, 297, 815
Houdashelt M. L., Bell R. A., Sweigart A. V., Wing R. F., 2000, AJ, 119, 1424
Ireland M. J., Scholz M., Wood P. R., 2011, MNRAS, 418, 114
Ita Y. et al., 2004, MNRAS, 347, 720
Ivezić Z., Nenkova M., Elitzur M., 1999, University of Kentucky Internal Report, User Manual for DUSTY. Available at http://www.pa.uky.edu/~moshe/dusty
Johnson H. L., Méndez M. E., 1970, AJ, 75, 785
Keller S. C., Wood P. R., 2006, ApJ, 642, 834
Kerschbaum F., Lebzelter T., Mekul L., 2010, A&A, 524, A87
Lombaert R. et al., 2013, A&A, 554, A142
Lucy L. B., 1967, Z. Astrophys., 65, 89
Nicholls C. P., Wood P. R., Cioni M.-R. L., Soszyński I., 2009, MNRAS, 399, 2063
Olivier E. A., Wood P. R., 2003, ApJ, 584, 1035
Ossenkopf V., Henning Th ., Mathis J. S., 1992, A&A, 261, 567
Pègouriè B., 1988, A&A, 194, 335
Rayner J. T., Cushing M. C., Vacca W. D., 2009, ApJS, 185, 289
Soker N., Clayton G. C., 1999, MNRAS, 307, 993
Soszyński I., 2007, ApJ, 660, 1486
Soszyński I., Udalski A., 2014, ApJ, 788, 13
Soszyński I., Wood P. R., 2013, ApJ, 763, 103
Soszyński I., Udalski A., Kubiak M., Szymański M., Pietrzyński G., Zebruń K., Szewczyk O., Wyrzykowski Ł., 2004, Acta Astron., 54, 129
Soszyński I. et al., 2007, Acta Astron., 57, 201
Soszyński I. et al., 2011, Acta Astron., 61, 217
Stello D. et al., 2014, ApJ, 788, L10
Stothers R. B., 2010, ApJ, 725, 1170
Tabur V., Bedding T. R., Kiss L. L., Giles T., Derekas A., Moon T. T., 2010, MNRAS, 409, 777
Takayama M., Saio H., Ita Y., 2013, MNRAS, 431, 3189
Tsuji T., 2000, ApJ, 538, 801

Van Hamme W., Wilson R. E., 2003, in Munari U., ed., ASP Conf. Ser. Vol. 298, Gaia Spectroscopy, Science and Technology. Astron. Soc. Pac., San Francisco, p. 323
van Loon J. Th., Cioni M.-R. L., Zijlstra A. A., Loup C., 2005, A&A, 438, 273
Wilson R. E., Devinney E. J., 1971, ApJ, 166, 605
Winters J. M., Fleischer A. J., Gauger A., Sedlmayr E., 1994, A&A, 290, 623
Wood P. R., Nicholls C. P., 2009, ApJ, 707, 573
Wood P. R. et al., 1999, in Le Bertre T., Lebre A., Waelkens C., eds, Proc. IAU Symp. 191, Asymptotic Giant Branch Stars. Astron. Soc. Pac., San Francisco, p. 151
Wood P. R., Olivier E. A., Kawaler S. D., 2004, ApJ, 604, 800

SUPPORTING INFORMATION

Additional Supporting Information may be found in the online version of this article:

Table 2. The time series data for a variable source in *J* band (OGLE-SMC-LPV-07852) (http://mnras.oxfordjournals.org/lookup/suppl/doi:10.1093/mnras/stv002/-/DC1).

Please note: Oxford University Press are not responsible for the content or functionality of any supporting materials supplied by the authors. Any queries (other than missing material) should be directed to the corresponding author for this paper.

This paper has been typeset from a TEX/LATEX file prepared by the author.